Heteroatom-Doped Graphene Nanoribbons as High-Performance Electrodes for Lithium-Ion Hybrid Supercapacitors

Bikash Ranjan Isaac [a †], Sakshi Patil [a †], Athira K. M. [a ‡], Athul K V [a ‡], S. Sreedeep [a] and Vijayamohanan K. Pillai [a]*

[a] Bikash Ranjan Isaac, Sakshi Patil, Athira, Athul K V, S. Sreedeep and Vijayamohanan K. Pillai

Department of Chemistry, Indian Institute of Science Education and Research, Tirupati Srinivasapuram, Yerpedu Mandal Tirupati Dist, Andhra Pradesh, India – 517619.

Email: vijay@iisertirupati.ac.in

Number of pages: 6

Number of figures: 5

Number of tables: 1

Cyclic Voltammetry

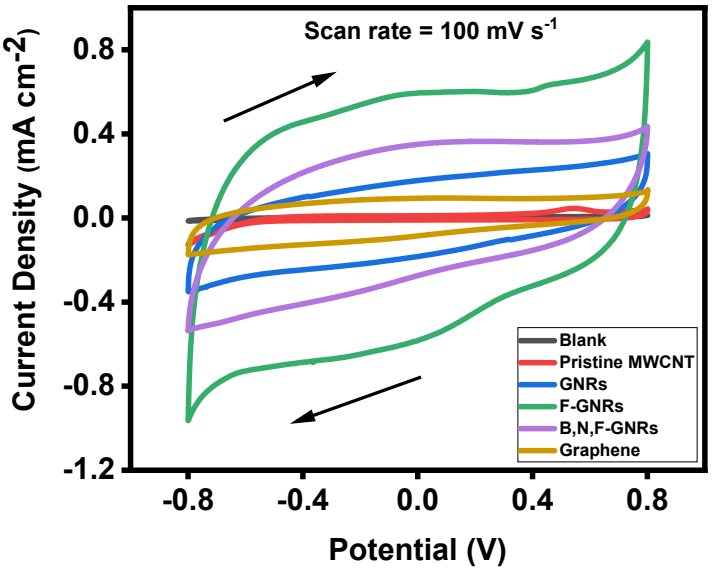

Figure S1. Cyclic voltammograms of pristine MWCNTs, electrochemically unzipped GNRs, F-GNRs, B, N, F–GNRs, and graphene in 1 M Na_2SO_4. Working electrode: glassy carbon modified with active material, counter electrode: Pt foil, reference electrode: $Hg/HgSO_4$, scan rate: 100 mV/s.

The cyclic voltammetry responses of the different carbon architectures clearly reflect the progressive structural and electronic modulation achieved through electrochemical unzipping, heteroatom functionalization/doping in Figure S1. The blank electrode displays a narrow, featureless profile typical of a purely capacitive background. Pristine MWCNTs show a slightly broadened loop arising from limited double-layer charging on curved graphitic surfaces. Upon unzipping, GNRs exhibit an enlarged and more rectangular voltammogram, consistent with higher accessible surface area, improved conductivity, and the exposure of abundant edge sites formed during longitudinal cleavage of the nanotube walls.[1] F-GNRs show the highest area in the capacitive current, reflecting the combined effect of defect-rich edges and the inductive electron-withdrawing nature of C–F bonds, which modulate charge distribution along the

ribbons.[2] The B,N,F-GNRs synthesized in ionic liquid show further enhancement due to synergistic heteroatom functionalization, which together promote superior ion accessibility and rapid interfacial charge transfer. Compared to graphene, all electrochemically engineered samples, especially F-GNRs and B,N,F-GNRs display substantially improved electrochemical reversibility, underscoring the advantage of room-temperature unzipping and controlled functionalization strategies for supercapacitor-grade carbon nanostructures.[3]

Rate Performance

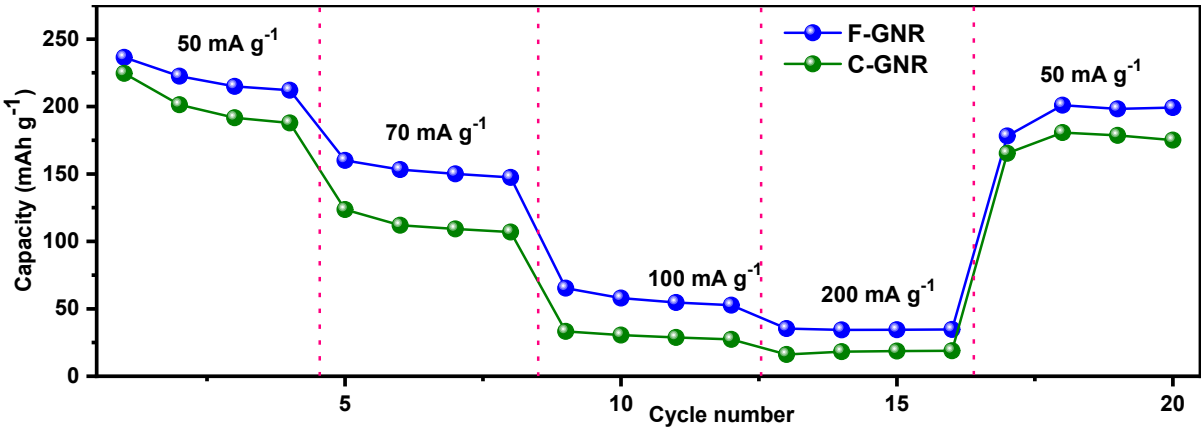

Figure S2. Plot showing the rate performance profile of GNRs and F-GNRs at different current densities of 50-200 mA g^{-1}.

Electrochemical Impedance Spectroscopy

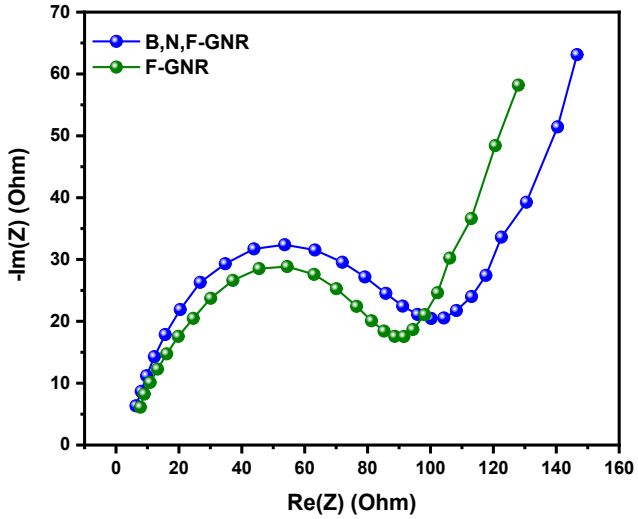

Figure S3. EIS spectra of B, N, F-GNRs and F-GNRs at 10th cycle.

Galvanostatic Charge-Discharge and cycling plot for B ,N ,F-Graphene Nanoribbon

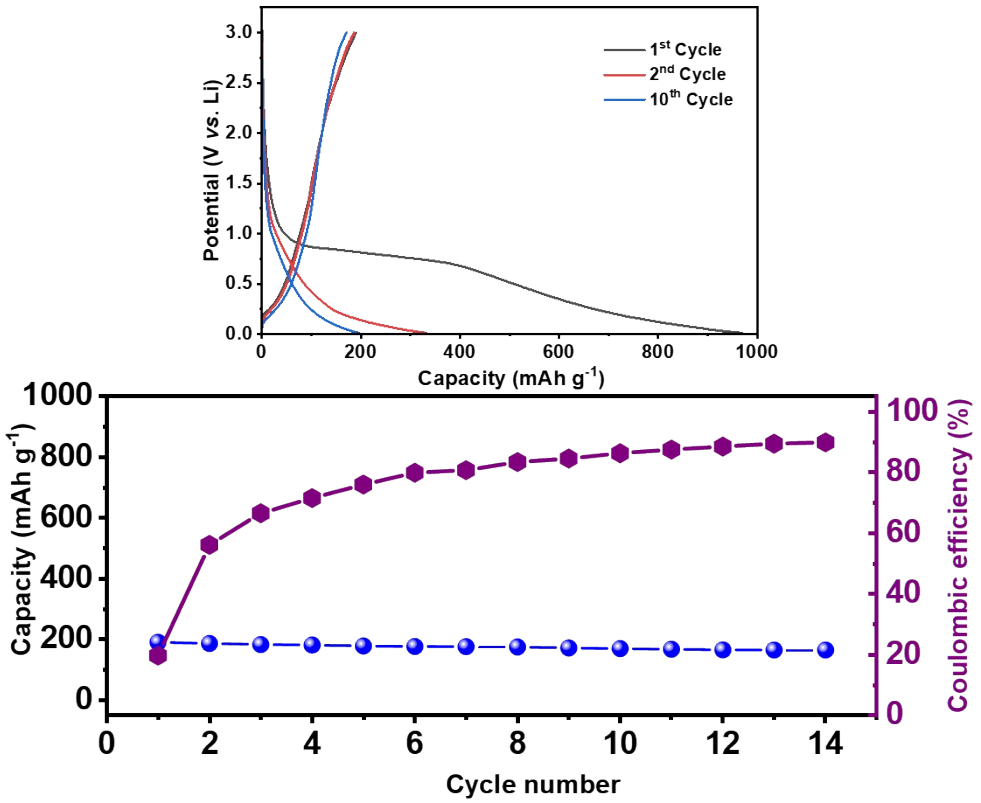

Figure S4. Galvanostatic charge–discharge profiles of the electrode recorded at a constant current density (100mA g-1), showing the 1st, 2nd, and 10th cycles and plot showing (a,b) the cycling profile of B ,N, F-GNRs.

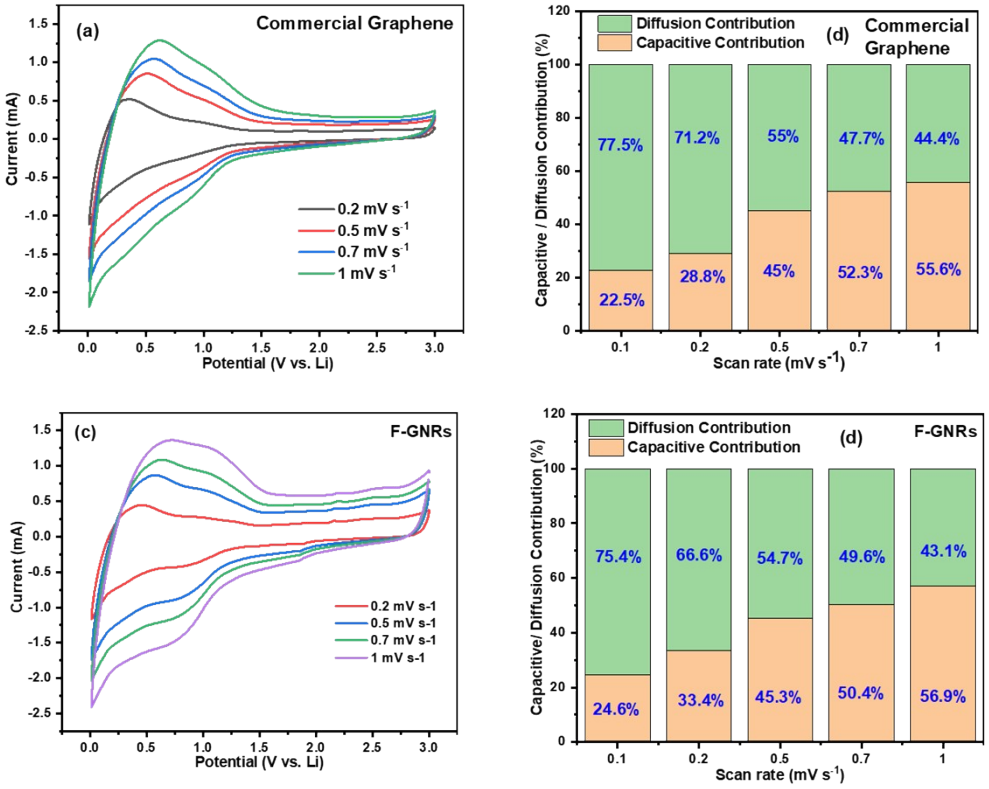

Figure S5. Plot showing the (a,b) CV curves of commercial graphene and its respective capacitive/diffusion contribution, (b,d) CV curves of F-GNRs and its respective capacitive/diffusion contribution at scan-rates ranging from 0.2-1 mV s-1 for the cell. Cycled in non-aqueous electrolyte.

Table S1. Various reported synthetic methods for graphene nanoribbons:

Methods	**Precursor**	**Capacity (mAh g^{-1})**	**Reference**
Graphene nanoribbons wrapping carbon-coated SnO_2 nanoparticles anchored on carbon nanotubes By hydrothermal method	MWCNTs	502	[4]
$Li_4Ti_5O_{12}$ GNRs using a solid-coating method	MWCNTs	142.3	[5]
Oxidation of arc discharge multi-walled MWCNTs	MWCNTs	344.73 (Full cell)	[6]
GNRs by electrochemical exfoliation	MWCNTs	242	This work
F-GNRs by electrochemical exfoliation	MWCNTs	342	This work
B, N, F-GNRs by electrochemical exfoliation	MWCNTs	330	This work

Table S1. Comparison of traditional benchmark GNRs with electro-synthesized GNRs.

Experimental Section

Electrolyte Source and Purity:

The electrolyte chemicals H_2SO_4 (Loba Chemie, purity ≥ 98 %), $BMIMBF_4$ (TCI, purity ≥ 98 %) CF_3SO_3H (TCI, purity ≥ 98 %). High-purity deionized (DI) water (resistivity ~18.2 MΩ·cm) obtained from a Millipore system was used for H_2SO_4 electrolyte preparations. Prior to use, the electrolyte solutions were freshly prepared and degassed to remove dissolved gases.

Electrode Pretreatment and Cleaning Procedure:

The working electrode Pt foil was mechanically polished using successive alumina slurries (1.0, 0.3, and 0.05 μm), followed by thorough rinsing with DI water and ultrasonication in ethanol and DI water (10 min each) to remove residual particles. The electrode was then dried under a nitrogen stream. The counter electrode Pt foil was cleaned by DI water washing. The reference electrode was calibrated prior to use.

Temperature Control:

The electrochemical synthesis was carried out at constant ambient laboratory temperature (25 ± 2 °C) without external heating. The experiments were performed under stable environmental conditions to avoid temperature-induced variations in reaction kinetics. This clarification has been explicitly added to the manuscript.

References:

1 D. B. Shinde, J. Debgupta, A. Kushwaha, M. Aslam and V. K. Pillai, *J. Am. Chem. Soc.*, 2011, **133**, 4168–4171.

2 S. S. Nair, B. R. Isaac, S. Alwarappan, S. Sreedeep and V. K. Pillai, *ACS Appl. Nano Mater.*, 2024, **7**, 7337–7344.

3 B. R. Isaac, S. Alwarappan and V. K. Pillai, *ACS Sustain. Chem. Eng.*, 2023, **11**, 16641–16649.

4 X. Li, X. Zhang, T. Li, X. Zhao and X. Zhang, *J. Alloys Compd.*, 2017, **729**, 1064–1071.

5 P. A. Medina 4th, H. Zheng, B. D. Fahlman, P. Annamalai, A. Swartbooi, L. le Roux and M. K. Mathe, *Springerplus*, 2015, **4**, 643.

6 J. Hernández-Ferrer, P. Laporta, F. Gutiérrez, M. D. Rubianes, G. Rivas and M. T. Martínez, *Electrochem. Commun.*, 2014, **39**, 26–29.